Supplementary Information (SI) for Nanoscale.

Supporting Information

Optimizing Active Sites via Chemical Bonding of 2D Metal-Organic Frameworks and MXene for Efficient Hydrogen Evolution Reaction

Anand P. Tiwari‡[1], Priyanshu Chandra‡[2], Md Saifur Rahman[1], Katherine A. Mirica[2] and William J. Scheideler*[1]

1. Thayer School of Engineering Dartmouth College, Hanover, NH 03755, United States
   E-mail: william.j.scheideler@dartmouth.edu
2. Department of Chemistry, Burke Laboratory, Dartmouth College, Hanover, New Hampshire 03755, United States

‡ These authors contributed equally

I. Materials and methods:

Tris(dibenzylideneacetone)dipalladium(0) ($Pd_2(dba)_3$), nickel(II) acetate tetrahydrate, triphenylene, and Ti_3AlC_2 (MAX phase) were purchased from Sigma-Aldrich or TCI Chemicals. Toluene, dichloromethane, acetone, and ethyl acetate were obtained from BDH Chemicals. Powder X-ray diffraction (PXRD) data was gathered using a Rigaku sixth-generation MiniFlex X-ray diffractometer with a 600 W (40 kV, 15 mA) CuKα (α = 1.54 Å) radiation source. Spectra are presented with the background subtracted and corrected for Kα. NMR spectra were recorded on a Bruker 600 MHz NMR spectrometer. Chemical shifts (δ) are expressed in ppm with tetramethylsilane (TMS) and solvent signals as internal references, and J values are given in Hz. Standard abbreviations indicating multiplicity were used as follows: s (singlet), br (broad), d (doublet), t (triplet), q (quartet), and m (multiplet). Scanning Electron Microscopy (SEM) was performed on a Thermo Scientific™ Helios™ 5 CX DualBeam instrument (Waltham, MA) equipped for X-ray analysis with Oxford Instruments Ultim Max 100 and Oxford Instruments Ultim Extreme 100 detectors (Abingdon, United Kingdom). Transmission electron microscopy (TEM) was performed on a Thermo Scientific Talos F200X G2 instrument. X-ray photoemission spectroscopy (XPS) analysis was conducted by Kratos Axis Supra XPS (X-ray Photoelectron Spectroscopy) system. Electrochemical characterization was performed with a VersaSTAT electrochemical workstation from Princeton Applied Research.

II. Synthesis and characterization of organic linker

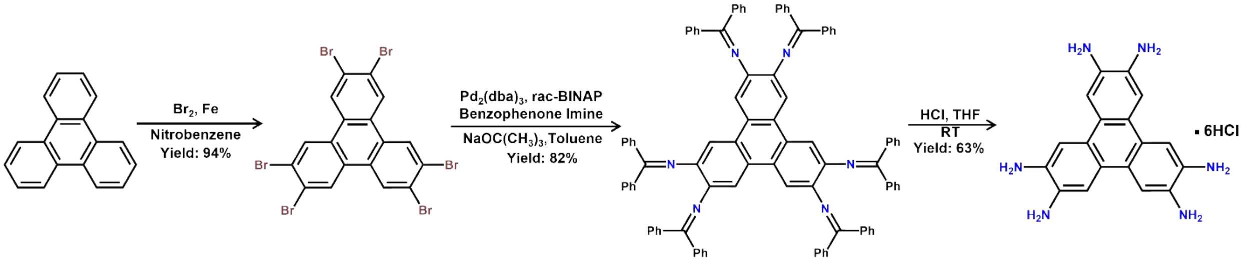

Figure S1. Synthetic scheme of triphenylene-2,3,6,7,10,11-hexaamine (HATP)

Step I: **synthesis of 2,3,6,7,10,11-hexabromotriphenylene**: A solution of 4.95 mmol triphenylene (1.15 g) in nitrobenzene (40 mL) was prepared in a round-bottomed flask. To this solution, iron powder (1.8 mmol, 100 mg) was added. Liquid bromine (43 mmol, 2.25 mL) was then added dropwise over the course of 15 minutes. The resulting mixture was stirred at room temperature for 24 hours, followed by refluxing at 205 °C for 2 hours. After allowing the reaction solution to cool to room temperature, diethyl ether (100 mL) was added, causing a solid precipitate to form. This solid was filtered and rinsed with diethyl ether (3 × 30 mL). The solid was then recrystallized in dichlorobenzene (60 mL). The resultant white solid was filtered, rinsed with diethyl ether (2 × 30 mL), and dried under reduced pressure at 70 °C. The final product, an off-white solid (3.2 g, yield = 94%), was used without further purification.

Step II: synthesis of N,N',N'',N''',N'''',N'''''-(triphenylene-2,3,6,7,10,11-hexayl)hexakis(1,1-diphenylmethanimine): To a flame-dried Schlenk flask purged with nitrogen was added tris(dibenzylideneacetone)dipalladium(0) (0.34 mmol, 310 mg) and racemic-BINAP (0.67 mmol, 425 mg). Degassed toluene (35 mL) was then added to the vessel, and the solution was subjected to four freeze-pump-thaw cycles, finally filling the vessel with nitrogen. The reaction mixture was heated to 110 °C for 30 minutes with stirring, and then allowed to return to room temperature. Under a positive pressure of nitrogen, the product from step I (1.45 mmol, 1.0 g), benzophenone imine (11 mmol, 1.9 mL), and sodium tert-butoxide (11 mmol, 1.1 g) were added. The solution was stirred at 110 °C for 18 hours under nitrogen, and then allowed to cool to room temperature. The reaction mixture was then diluted with dichloromethane (40 mL) and filtered over a pad of Celite, rinsing with an additional 50 mL of dichloromethane. The filtrate was concentrated under reduced pressure and purified by column chromatography using an eluent of 1:8 ethyl acetate. The bright orange product (1.75 g, yield = 83%) was isolated and dried under reduced pressure.

Step III: synthesis of triphenylene-2,3,6,7,10,11-hexaamine (HATP): The product from step II (0.33 mmol, 430 mg) was dissolved in tetrahydrofuran (33 mL), and 2.0 M hydrochloric acid (4 mmol, 1.0 mL) was added slowly. Upon the addition of the acid, an immediate color change was observed (orange to red), and a precipitate began to form. The mixture was stirred at room temperature for 30 minutes, after which the fine white powder precipitate was isolated by centrifugation. This solid was washed with tetrahydrofuran (10 mL) and dried under vacuum, yielding 90 mg (63%). The characterization of the product matched the literature[1].

$Ni_3(HITP)_2$ MOF synthesis: HATP (30 mg, 0.1 mmol) was dissolved in 10 mL of water. Nickel acetate tetrahydrate (50 mg, 0.2 mmol) in 15 mL of water was added to the solution. The mixture was sonicated for 5 minutes and then heated at 70 °C for 24 hours in a 100 mL round-bottom flask without capping it. After the reaction was completed, the resulting dark powder was collected by vacuum filtration. The solid was washed with water (3 × 15 mL) and ethanol (3 × 15 mL), then dried under vacuum overnight.

For activation, the MOF powder was immersed in 20 mL of deionized (DI) water for 24 hours, with the water being exchanged every few hours. The powder was then immersed in 20 mL of ethanol for 24 hours, with the ethanol being exchanged every few hours. Finally, the powder was dried under vacuum at 70 °C for 24 hours. Characterization of $Ni_3(HITP)_2$ MOF by powder X-ray diffraction (PXRD) indicates bulk phase crystallinity, as characteristic peaks corresponding to the (100), (200), and (001) planes are present in the synthesized sample and match well with the simulated PXRD pattern (Figure S2 (a)). Scanning electron microscopy (SEM) characterization of $Ni_3(HITP)_2$ MOF reveals the presence of rod-shaped morphology in the MOF crystals, which is consistent with earlier reports (Figure S2 (b)).

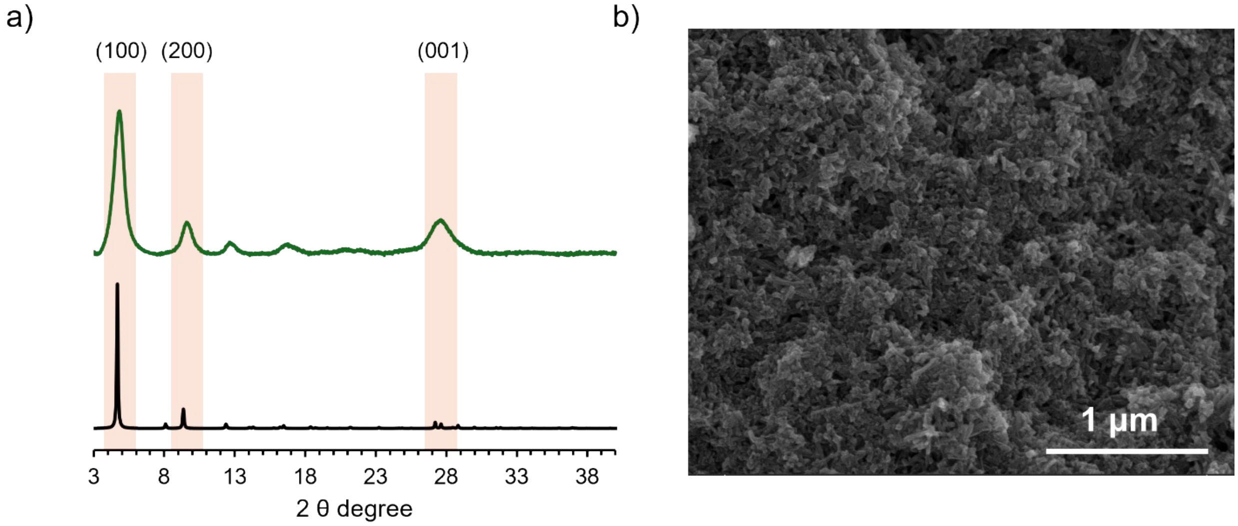

Figure S2. Characterization of $Ni_3(HITP)_2$ MOF by (a) powder x-ray diffraction (PXRD), and (b) scanning electron microscopy (SEM)

Synthesis of Pristine-$Ti_3C_2T_X$ (MXene Phase): $Ti_3C_2T_X$-MXene was synthesized according to the procedure outlined in our previous report[2]. Briefly, 1 g of Ti_3AlC_2 powder was added in a solution composed of 3 ml of 47–49% concentrated HF, 6 ml of 47–49% concentrated HCl, and 1 ml of deionized (DI) water. The mixture was stirred for 24 hours at room temperature. After stirring, the mixture was washed with DI water until the pH reached 7 and separated by centrifugation. For exfoliation, 8 M $LiCl_6$ was added to DI water in a 7:3 ratio in the MXene solution and stirred for 4 hours. Afterward, the $LiCl_6$ was washed, and the solution was centrifuged to separate the nanosheets from the supernatants.

Templated growth of $Ni_3(HITP)_2$@MXene: For in situ growth of $Ni_3(HITP)_2$MOF on MXene, we use four different conditions 1) 10 mg HATP and 5mg MXene in 10 mL DI water (MOF@$Ti_3C_2T_x$(66%HATP)), 2) 10 mg HATP and 10mg MXene in 10 mL DI water (MOF@$Ti_3C_2T_x$(50%HATP)), 3) 10 mg HATP and 15mg MXene in 10 mL DI water (MOF@$Ti_3C_2T_x$(33%HATP),, and 4) 10 mg HATP and 20mg MXene in 10 mL DI water (MOF@$Ti_3C_2T_x$(25%HATP)).

For a typical synthesis under condition #1, 5 mg of MXene is dispersed in 5 mL of deionized (DI) water and sonicated for 30 minutes in a 20 mL drum vial. Nickel acetate tetrahydrate (15 mg, 0.06 mmol) is then added to this dispersion, followed by the addition of HATP (10 mg, 0.03 mmol) dissolved in 5 mL of DI water. The resulting mixture is sonicated for an additional minute. Sodium acetate (82 mg, 1 mmol) is subsequently added to the mixture, which is sonicated for another minute. This reaction mixture is then heated at 70 °C for 24 hours with the vial loosely capped.

After the reaction is complete, the precipitate is separated by vacuum filtration and washed with DI water (3 × 20 mL) and ethanol (3 × 20 mL). For activation, the same procedure used for the MOF was followed: the MOF-MXene composite was immersed in 20 mL of DI water for 24 hours, with the water being exchanged every few hours. The composite was then immersed in 20 mL of ethanol for 24 hours, with the ethanol being exchanged every few hours. Finally, the composite was dried under vacuum at 70 °C for 24 hours.

Electrochemical Characterization: Firstly, 4 mg of the synthesized $Ni_3(HITP)_2$@Mxene were suspended in a solution containing 660 µL of DI water, 220 µL of ethanol, and 80 µL of Nafion 117 solution. Then, 3 µL of the prepared solution was dropped onto a glassy carbon electrode (d = 3 mm). Electrocatalytic performances were analyzed with a three-electrode systems (working electrode was as-prepared samples on glassy carbon electrode, the reference electrode was Ag/AgCl in 3M KCl, and the counter electrode was a Pt wire in 0.5 M H_2SO_4 and 1.0 M KOH electrolytes. All potentials were converted to the Reversible Hydrogen Electrode (RHE) scale using the formula:

$$E_{(RHE)} = E_{Ag/AgCl} + 0.059\ pH + E^{o}_{Ag/AgCl},\ \text{where } E^{o}_{Ag/AgCl} = 0.1976\ V$$

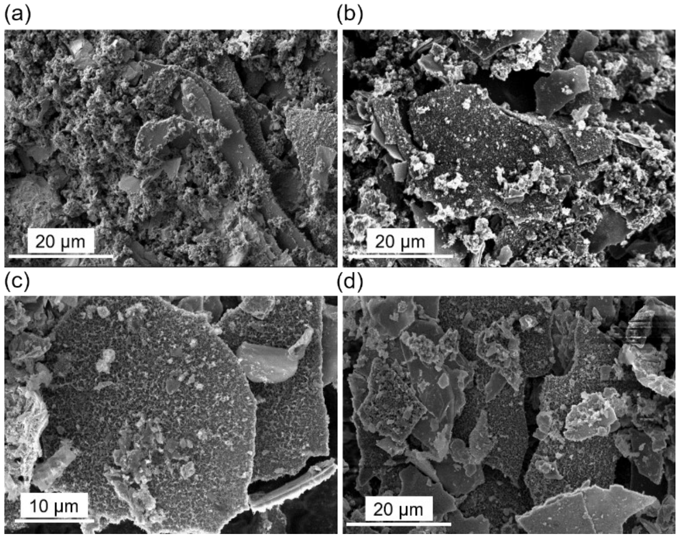

Figure S3. SEM images of (a) MOF@$Ti_3C_2T_x$(66%HATP), (b) MOF@$Ti_3C_2T_x$(50%HATP), (c) MOF@$Ti_3C_2T_x$(33%HATP), (d) MOF@$Ti_3C_2T_x$(25%HATP).

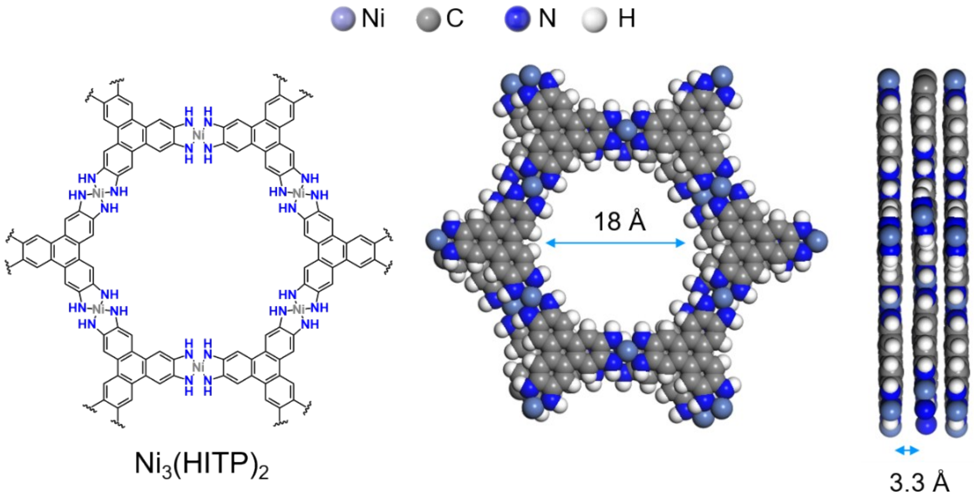

Figure S4. Schematic illustration of chemical and atomic structure of $Ni_3(HITP)_2$.

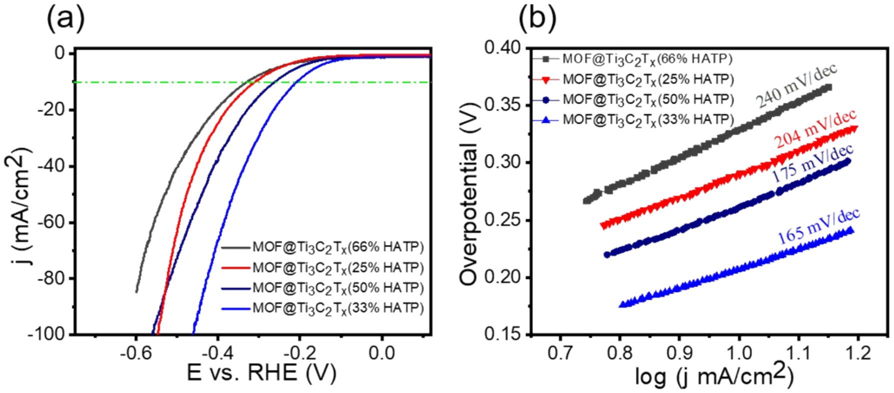

Figure S5. Electrocatalytic performance for HER of different unannealed compositions of MOF and MXene in 1.0 M KOH. (a) Linear sweep voltammetry. (b) Tafel plots.

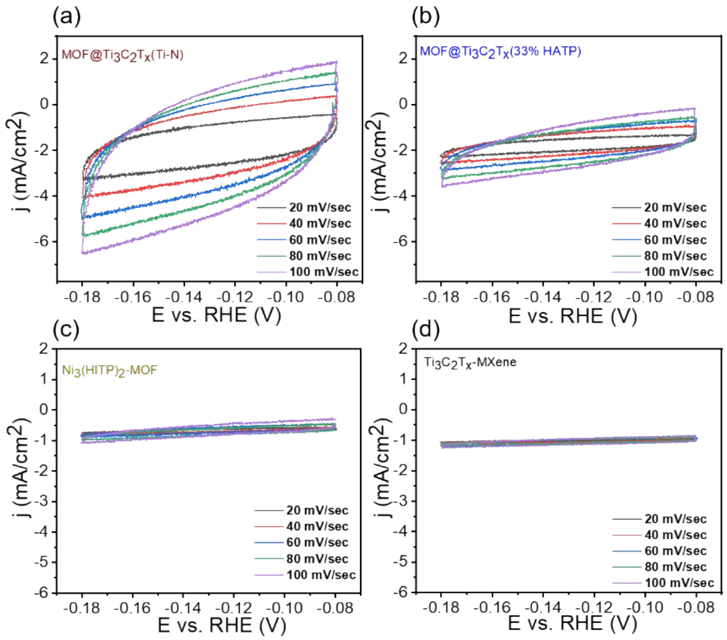

Figure S6. Cyclic voltammetry of $Ni_3(HITP)_2@Ti_3C_2T_x$ in 1.0 M KOH: (a) MOF@$Ti_3C_2T_x$(Ti-N), (b) MOF@$Ti_3C_2T_x$(33%HATP), (c) $Ni_3(HITP)_2$-MOF, and (d) $Ti_3C_2T_x$-MXene.

Description to calculate turn over frequency (TOF) for H_2:

The structural data of $Ti_3C_2T_x$ as follows:

Density of $Ti_3C_2T_x$ = 4.21 g cm^{-3}. Average size of nanoparticle (determined from the Scherrer equation) = 15 nm. The shapes of the nanoparticles are approximated to spherical.

Loading amount of MXene on the electrode is 1 mg/cm^2.

Total volume of $Ti_3C_2T_x$ particles present on the electrode

$$= (1\times10^{-5}) / 4.21 = 2.4\times10^{-6}\ cm^3 \qquad (S1)$$

Total number of $Ti_3C_2T_x$ nanoparticles present on the electrode

$$= (2.4\times10^{-6}) / [(4/3)(\pi)(r^3)] \qquad (S2)$$

$$= (2.4\times10^{-6}) / [4.18\times(7.5\times10^{-7})^3]$$

$$= 1.3\times10^{12}\ \text{particles}$$

Surface area of one $Ti_3C_2T_x$ nanoparticle

$$= (4)(\pi)(r^2) \qquad (S3)$$

$$= 0.70\times10^{-15}\ m^2$$

Total surface area of all $Ti_3C_2T_x$ the nanoparticles present

$$= (1.3\times10^{12})\times(0.70\times10^{-15}) = 9.1\times10^{-4}\ m^2 \quad (S4)$$

The area of per unit cells of $Ti_3C_2T_x = 2.10\times10^{-19}\ m^2$ (S5)

There are 3.5 Ti atoms in this unit cell.

Hence, the total number of surface Ti atoms present

$$= [3.5 / (2.1\times10^{-19}\ m^2)]\times(9.1\times10^{-4}\ m^2) \qquad (S6)$$

$$= 1.6\times10^{16}\ \text{atoms}$$

We assume that all the surface Ti atoms participate in the HER. Hence, the turnover frequency of H_2 production at Overpotentials = 180 mV (current density measured = 10 mA cm^{-2}, electrolyte = 1.0 M KOH).

$$= [(10\ mA/cm^2)(10^{-3})(0.196\ cm^2)(6.02\times10^{23})] / [(96485.3\ C/mol)(2)(1.6\times10^{16})] \quad (S7)$$

$$= 0.37\ s^{-1}$$

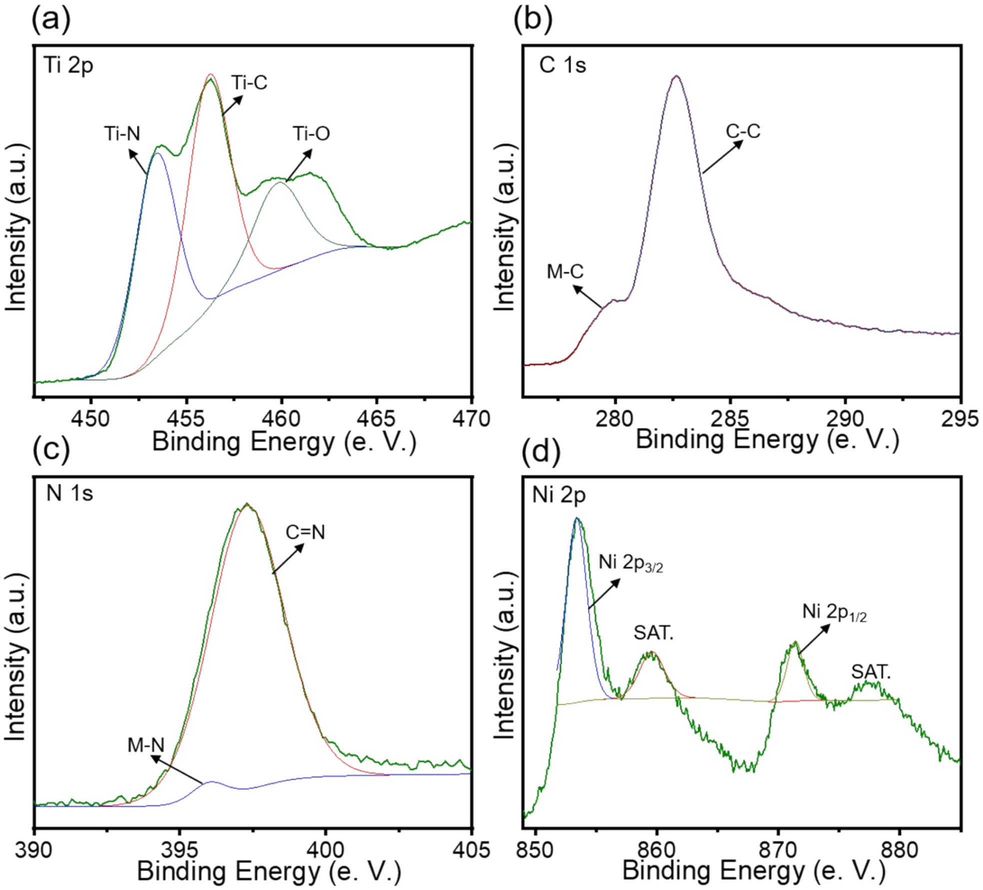

Figure S7. High-resolution XPS spectra with fitting curves of (a) Ti 2p, (b) C 1s, (c) N 1s, and (d) Ni 2p for MOF@$Ti_3C_2T_x$ (Ti-N) after a 150-hour stability test at 20 mA/cm^2 in 1.0 M KOH.

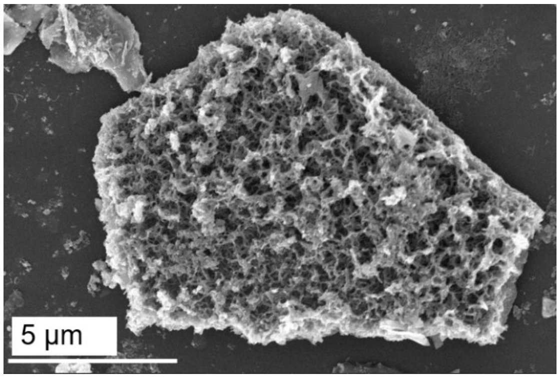

Figure S8. High-resolution SEM image of MOF@$Ti_3C_2T_x$ (Ti-N) after a 150-hour stability test at 20 mA/cm^2 in 1.0 M KOH.

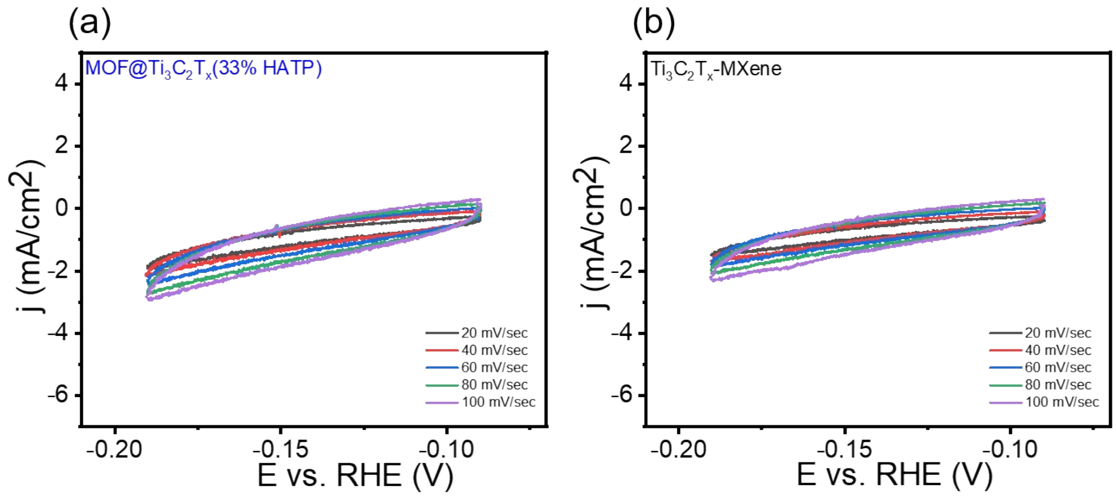

Figure S9. Cyclic voltammetry of (a) MOF@$Ti_3C_2T_x$(33%HATP), and (b) $Ti_3C_2T_x$-MXene in 0.5 M H_2SO_4.

Table S1. Comparision of electrocatalytic activity of MOF@$Ti_3C_2T_x$(Ti-N) with reported MOFs

MOF	Electrolyte	Overpotentials	References
ZIF-8 derived MoC	1 M KOH	182 mV	*Advanced Materials*, 2019, **31**, 1900699[3]
$Cu_3(HHTP)_2$	1 M KOH	273 mV	*Science Advances,* 2021, **7**, eabg2580[4]
Co/Cu-MOF	1 M KOH	567 mV	*International Journal of Hydrogen Energy,* 2020, **45**, 11077–11088[5]
CoNi-MOF	1 M KOH	265 mV	*Advanced Materials Interfaces,* 2018, **5**, 1800849[6]
Ni-ZIF/NiB@NF-4	1 M KOH	234 mV	*Advanced Energy Materials,* 2020, **10**, 1902714[7]
NiFe-MOF/NF	1 M KOH	240 mV	*Nat Commun,* 2017, **8**, 15341[8]
CoS_2@MOF	1 M KOH	232 mV	*Electrochimica Acta*, 2023, **458**, 142511[9]
CoNi-MOF	1 M KOH	313 mV	*Journal of Alloys and Compounds*, 2023, **931**, 167575[10]
NSQDs@NiFe-MOF	1 M KOH	219 mV	*Inorg. Chem. Front.*, 2023, **10**, 1294–1304[11]
Pr-MOF/Fe_2O_3	1 M KOH	238 mV	*Heliyon*, 2023, **9**, e20261[12]
2D NiCo/NH_2-UiO-66 MOF	1 M KOH	224 mV	*J. Mater. Chem. A*, 2023, **11**, 10309–10318[13]
Fe/Co-BDC	1 M NaOH	188 mV	*Journal of Energy Storage*, 2023, **61**, 106702[14]
Co/Fe MOF_Se	1 M KOH	235 mV	*Front. Energy*, 2024, **18**, 378–389[15]
MOF@$Ti_3C_2T_x$(Ti-N)	**1 MKOH**	**180 mV**	**This work**

References:

1 M. K. Smith and K. A. Mirica, *J. Am. Chem. Soc.*, 2017, **139**, 16759–16767.

2 A. P. Tiwari, S. McBride, A. B. Hamlin, M. S. Rahman, J. E. Huddy, G. Hautier and W. J. Scheideler, *ACS Sustainable Chem. Eng.*, 2023, **11**, 12084–12092.

3 X. F. Lu, L. Yu, J. Zhang and X. W. (David) Lou, *Advanced Materials*, 2019, **31**, 1900699.

4 W. Cheng, H. Zhang, D. Luan and X. W. (David) Lou, *Science Advances*, 2021, **7**, eabg2580.

5 Q. Qiu, T. Wang, L. Jing, K. Huang and D. Qin, *International Journal of Hydrogen Energy*, 2020, **45**, 11077–11088.

6 M. Liu, W. Zheng, S. Ran, S. T. Boles and L. Y. S. Lee, *Advanced Materials Interfaces*, 2018, **5**, 1800849.

7 H. Xu, B. Fei, G. Cai, Y. Ha, J. Liu, H. Jia, J. Zhang, M. Liu and R. Wu, *Advanced Energy Materials*, 2020, **10**, 1902714.

8 J. Duan, S. Chen and C. Zhao, *Nat Commun*, 2017, **8**, 15341.

9 G. Zhang, J. Wang, Y. Xie, Y. Shao, Y. Ling, Y. Chen and Y. Zhang, *Electrochimica Acta*, 2023, **458**, 142511.

10 S. Chen, W. Liang, X. Wang, Y. Zhao, S. Wang, Z. Li, S. Wang, L. Hou, Y. Jiang and F. Gao, *Journal of Alloys and Compounds*, 2023, **931**, 167575.

11 J. Lin, H. Zhou, R. S. Amin, A. E. Fetohi, K. M. El-Khatib, C. Wang, L. Guo and Y. Wang, *Inorg. Chem. Front.*, 2023, **10**, 1294–1304.

12 B. Shabbir, K. Jabbour, S. Manzoor, M. F. Ashiq, K. F. Fawy and M. N. Ashiq, *Heliyon*, 2023, **9**, e20261.

13 S. Sk, R. Madhu, D. S. Gavali, V. Bhasin, R. Thapa, S. N. Jha, D. Bhattacharyya, S. Kundu and U. Pal, *J. Mater. Chem. A*, 2023, **11**, 10309–10318.

14 R. Nivetha, J. Jana, S. Ravichandran, H. N. Diem, T. Van Phuc, J. S. Chung, S. G. Kang, W. M. Choi and S. H. Hur, *Journal of Energy Storage*, 2023, **61**, 106702.

15 Z. Shang, T. Li, B. Hu, M. Liu, W. Lu, F. Yu and Y. Zheng, *Front. Energy*, 2024, **18**, 378–389.